PCCP

Accepted Manuscript

This article can be cited before page numbers have been issued, to do this please use: D. Marchione and M. R. S. McCoustra, *Phys. Chem. Chem. Phys.*, 2016, DOI: 10.1039/C6CP01787H.

ROYAL SOCIETY OF CHEMISTRY

www.rsc.org/pccp

View Article Online
DOI: 10.1039/C6CP01787H

Journal Name

ARTICLE TYPE

Cite this: DOI: 10.1039/xxxxxxxxxx

Non-covalent Interaction of Benzene with Methanol and Diethyl Ether Solid Surfaces†

Demian Marchione,*[a,b] and Martin R. S. McCoustra[a]

Received Date
Accepted Date

DOI: 10.1039/xxxxxxxxxx

www.rsc.org/journalname

We present laboratory experiments on binary, layered ices comprised of benzene (C_6H_6) on methanol (CH_3OH) and on diethyl ether ($CH_3CH_2OCH_2CH_3$). Temperature programmed desorption (TPD) and reflection-absorption infrared spectroscopy (RAIRS) have been used to investigate the growth mechanisms in these systems. *Ab initio* quantum chemical calculations on simple gas-phase model clusters are used to aid interpretation of the experimental data by highlighting the key interactions established at the interface. Our observations are consistent with C_6H_6 forming islands on CH_3OH, although evidence of strong hydrogen bonding interactions indicates some degree of surface wetting. In contrast, layer-by-layer growth is proposed for C_6H_6 on the $CH_3CH_2OCH_2CH_3$ substrate.

1 Introduction

Non-covalent interactions play a crucial role in many natural phenomena. Experimental and theoretical studies[1] have highlighted how such interactions affect the properties of gas phase[2–7] systems, liquids[8–11] and molecular crystals.[12,13] A great deal of attention has been given to hydrogen bonding interactions involving aromatic π-systems because of their ubiquitous presence in biological systems,[14–16] where they are a key factor in determining the three-dimensional structure of proteins and other biopolymers, and in supramolecular chemistry[17–19] where they determine the selectivity of molecular recognition processes.[20–23]

As a prototypical system, benzene-water (C_6H_6-H_2O) complexes have been extensively studied theoretically and experimentally and have been shown to display two different types of hydrogen bonds as the aromatic molecule can act either as an hydrogen bond acceptor or as an hydrogen bond donor. In the former case, the π-electron density interacts with the OH group of H_2O, while in the latter case the C_6H_6 molecules bind with the lone pair of the O-atom, *via* a CH···O interaction.[24–34] Weaker interactions of C_6H_6 with other molecules, such as methane (CH_4), ammonia (NH_3), methanol, (CH_3OH), and dimethyl ether (CH_3OCH_3), are also possible and have been reported.[11,35–37]

In this context, our study focusses on two systems: C_6H_6-CH_3OH, and C_6H_6-$CH_3CH_2OCH_2CH_3$ (benzene-diethyl ether), and their comparison with our existing measurements on C_6H_6-H_2O. In essence, we have reduced the degree of hydrogen bonding in the substrate film and possibly between C_6H_6 and the substrate by substituting the hydrogen atom (H) for an alkyl group. The choice of the heavier ethyl group in the ether substrate was purely due to technical limitations in our experiment.

These particular species were also chosen because of their astrophysical interest. C_6H_6 is thought to form in the interstellar medium (ISM) under single collision conditions *via* the gas phase reaction of ethynyl radicals with 1,3-butadiene,[38] and has been detected in protoplanetary nebula.[39] It is also efficiently produced by ion chemistry in the upper atmosphere of Titan.[40,41] C_6H_6 is proposed as the starting point for the generation of polycyclic aromatic hydrocarbons (PAHs)[42,43] which carry a significant proportion of the interstellar carbon budget, although the efficiency of such synthetic route is still debated.[44,45] Such is the universality of C_6H_6 and the PAHs that their deposition on solid-state materials (grains and ices) in the astrophysical environment is inevitable and laboratory investigations of such are therefore warranted.

[a] Institute of Chemical Sciences, Heriot-Watt University, EH14 4AS, Edinburgh, UK.

[b] Present address: Science Division, Jet Propulsion Laboratory, California Institute of Technology, Pasadena, CA 91109, USA.
E-mails: dmarchio@caltech.edu or marchionedemian@gmail.com (D. Marchione), and m.r.s.mccoustra@hw.ac.uk (M.R. S. McCoustra)

† Electronic Supplementary Information (ESI) available: [details of any supplementary information available should be included here]. See DOI: 10.1039/b000000x/

View Article Online
DOI: 10.1039/C6CP01787H

Solid H_2O, both in the form of compact amorphous solid water (c-ASW) and as crystalline ice, is the most abundant species detected in solid phase in the ISM. In the densest regions of the ISM, carbon monoxide (CO) freeze out can occur on the water ice surface. Hydrogenation of CO by H atoms efficiently produces CH_3OH, which is one of the two most abundant simple organic molecules in the solid state in the ISM along with CH_4.[46] In contrast, the presence in the icy mantles of complex ethers including $CH_3CH_2OCH_2CH_3$ has not been confirmed. Solid state photochemical mechanisms in cold, dense gas and gas phase mechanisms following ice evaporation in hot cores have both been proposed.[47] However, in the present situation, this molecule represents a convenient system to investigate weak non-covalent interactions with the π-electron density of C_6H_6 while keeping a logical continuity with H_2O and CH_3OH.

The interaction between C_6H_6 and ASW ice surfaces has been studied with vibrational spectroscopy,[48] time-of-flight secondary ion mass spectrometry,[49] metastable impact electron spectroscopy,[50] and temperature programmed desorption (TPD).[51] However, as far as we are aware, there are no studies of C_6H_6 adsorption on CH_3OH or $CH_3CH_2OCH_2CH_3$ surfaces under ultra-high vacuum (UHV) conditions.

In this paper, we present data for C_6H_6 adsorbed on top of a thick ice of CH_3OH or $CH_3CH_2OCH_2CH_3$. This work is a prerequisite to a full investigation of the role of hydrogen bonding in enabling the transfer of electronic excitation to interfaces promoting desorption in astrophysical solids subject to cosmic ray interactions extending our previous work on the C_6H_6/H_2O system.[28,29,52]

2 Methods

2.1 Experimental

The experiments discussed here were performed in a stainless steel UHV chamber that has been described in detail elsewhere.[51,53] A combination of liquid-nitrogen-trapped diffusion pumps and a titanium sublimation pump allows to reach a base pressure in the chamber of $2 < 10^{-10}$ Torr at room temperature. The substrate is a polished stainless steel disk cooled by a liquid nitrogen in a reservoir in thermal contact with the sample mount giving a base temperature of 109 ± 2 K. The substrate was resistively heated to 500 K for 15 minutes to remove volatile contaminants before cooling prior to conducting experiments each day. A K-type thermocouple, welded to the edge of the disk, was employed for temperature monitoring with a precision of 0.5 K. Layered ices were obtained by sequential background deposition using C_6H_6 (Fluka 99.5% pure), CH_3OH (Sigma-Aldrich, HPLC grade 99.9% pure), or $CH_3CH_2OCH_2CH_3$ (Sigma-Aldrich ,Chromasolv grade 99.9% pure). All the chemicals were stored in separate glass vials and were further purified by several freeze-pump-thaw cycles before use. Cross-contamination was minimised by collecting the vapour phase from the liquids using two independent manifolds each interfaced to its own dedicated fine-control leak valve (Vacuum Generators MD95). Exposure is reported in Langmuir units (1 L = 10^{-6} Torr s). Film thickness (d) can be estimated from:

$$d = \frac{SPt}{\sqrt{2\pi m k_B T}} \frac{1}{\rho_s} = \frac{Z_W t}{\rho_s} \quad (1)$$

where S is the sticking coefficient assumed to be 1, P is the pressure recorded on the hot cathode ion gauge corrected for the approximate molecular ionisation efficiencies[§],[54–57] t is the time of exposure, k_B is the Boltzmann constant, T is the temperature for the dosed molecules, Z_W is the bombardment rate (the incident flux), ρ_S is the molecular volume density and m is the mass. In the expression, we first define the number of molecules deposited onto the substrate (molecules per unit of surface area) during the dose and then divide this by the density (molecules per unit of volume). In particular, we assumed that the densities of the molecular solids are 1.91×10^{22} molecule cm^{-3}, 5.80×10^{21} molecule cm^{-3}, and 8.57×10^{21} molecule cm^{-3} for CH_3OH,[58] $CH_3CH_2OCH_2CH_3$,[¶] and C_6H_6[59] respectively.

Desorption of the species, during linear heating in TPD experiments, was followed by a crossed-beam source, quadrupole mass spectrometer (VG Microtech PC300D, further modified by European Spectrometry Systems) with a homemade line-of-sight tube facing the front of the sample. RAIR spectra were recorded using an FTIR spectrometer (Nicolet 870) with the co-addition of 1024 scans at a resolution of 2 cm^{-1}.

2.2 Computational Details

All calculations, including the evaluation of the equilibrium geometries, single points (SP), and vibrational frequency analysis were performed using Gaussian 09[60] thanks to the EPSRC UK National Service for Computational Chemistry Software (NSCCS) at Imperial College London. All the systems were optimised, with no symmetry constrains, using the Møller-Plesset second order approach (MP2)[61,62] with a Dunning's augmented correlation-consistent polarised valance double-zeta basis set (aug-cc-pVDZ) followed by a single point (SP) calculation employing the aug-cc-pVTZ basis set.[63–65] Further corrections for higher-order correlations beyond the MP2 method were considered with SP calculations using singles and doubles coupled cluster theory with perturbative treatment of triple excitations, CCSD(T), for all the two-molecule complexes. The correction energy term, ΔCCSD(T), was calculated from the difference of SP energies at CCSD(T)/cc-pVDZ and MP2/cc-pVDZ level assuming this to be independent on the basis set size[37,66] and reducing the computational cost. In

§ 1.87 for CH_3OH, 5.1 for $CH_3CH_2OCH_2CH_3$, and 6.0 for C_6H_6
¶ Density of the liquid phase, Sigma-Aldrich

View Article Online
DOI: 10.1039/C6CP01787H

contrast, due to the steep scaling of coupled-cluster methods the systems with more than two molecules where only investigated using MP2 perturbation theory as detailed above. Basis set superposition error (BSSE) corrections were made using the function counterpoise (CP) method[67,68] for all the calculations.

The systems investigated are two-molecule complexes or larger clusters. In the latter case, CH_3OCH_3 was used instead of $CH_3CH_2OCH_2CH_3$ in order to simplify the calculations by reducing the number of degrees of freedom and the CPU cost while retaining the type of interactions existing between the larger ether and the aromatic molecule. *Ab initio* calculations were performed only for selected configurations for clusters containing more than two molecules. Molecules were visualised using Molden 5.1.[69]

Finally, harmonic vibrational frequency analysis was performed at MP2/6-31G(d,p) level for each of the optimised structures. No imaginary frequencies were found, and hence all the computed complexes can be regarded as minima and not saddle points with respect to the employed theoretical approach.

3 Results and Discussion

We first present data from TPD and reflection-absorption infrared (RAIR) measurements of C_6H_6 adsorbed on top of a thick ice of CH_3OH or $CH_3CH_2OCH_2CH_3$. The analysis of TPD traces provides an insight into the C_6H_6 film growth mechanism and allows us to estimate the adsorption energy at sub-monolayer coverages. RAIR spectroscopy was employed to provide a qualitative description about the interactions established at the interface. Comparison with previously published work on C_6H_6 on c-ASW is made.

In addition, we have performed quantum mechanical (QM) calculations to provide for a consistent analysis on simple systems that has the sole scope of highlighting the type of intermolecular forces in play, confirming the energetics and the trends observed experimentally in the solid phase. This comparison can be somehow justified on the basis that the assembly and the aggregation of hydrophobic units (*e.g.* C_6H_6 in H_2O) is driven enthalpically for large clusters,[10,70–73] and hence the interplay at the equilibrium between the possible intermolecular interactions in complexes containing few molecules (calculations) can be translated to macroscopic systems (experiments).

We first present a systematic analysis of simple two-molecule complexes of C_6H_6-H_2O, C_6H_6-CH_3OH, C_6H_6-CH_3OCH_3 and C_6H_6-$CH_3CH_2OCH_2CH_3$. Then, the fundamental interactions existing between the two species are explored in larger clusters comprising three or four molecules. Previous studies have reported the main equilibrium arrangements for C_6H_6 with several molecules of H_2O or CH_3OH.[11,31–34,74] However, the value of the current analysis lies in the consistency of the level of theory used for all the investigated systems, and the addition of studies on C_6H_6-$CH_3CH_2OCH_2CH_3$ and C_6H_6-$(CH_3OCH_3)_2$ clusters that have not been reported as to date. Clearly, the C_6H_6-$CH_3CH_2OCH_2CH_3$ system is the most challenging complex to describe, thus it sets the minimum level of theory that guarantees consistency, and a satisfactory accuracy to model the intermolecular interactions. Amicangelo *et al.*[37] successfully investigated the analogous complex of C_6H_6 with the simpler CH_3OCH_3 and so we have based our calculations on a similar level of theory and method.

3.1 TPD and RAIRS of C_6H_6/CH_3OH

Fig. 1 displays the TPD data corresponding to very low exposures of C_6H_6 on a thick film of CH_3OH (15.2 nm). It is important

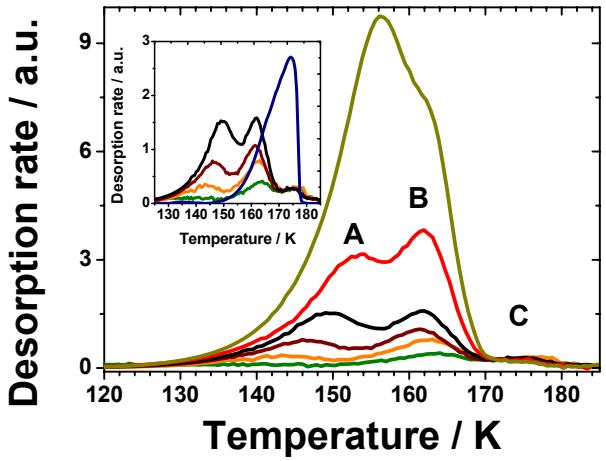

Fig. 1 TPD traces for C_6H_6 desorption from a thick ice of CH_3OH (200 L). C_6H_6 exposures displayed are 0.01 L in green, 0.02 L in orange, 0.05 L in brown, 0.1 L in black, 0.2 L in red, 0.5 L in dark yellow. There are three distinctive features: a low temperature peak (A), a high temperature peak (B) and a shoulder (C). The inset highlights the lower coverages TPD traces up to 0.1 L and includes the scaled desorption profile of CH_3OH (in blue).

to stress that all the C_6H_6 TPD data correspond to coverages in the sub-monolayer regime, up to 5×10^{-2} equivalent monolayers (ML)*. Three distinctive peaks can be observed: a low temperature peak (A) between 140 K and 155 K, a high temperature peak (B) between 160 K and 170 K and a shoulder (C) above 170 K that is already saturated at 0.01 L as highlighted in the inset. The feature labelled as C displays a striking match with the falling edge of the CH_3OH TPD trace, and hence, can be explained as co-desorption of C_6H_6 with CH_3OH. The interpretation of the two main peaks is not as straightforward because of the intrinsic complexity of the system that resulted in little reproducibility of the data. In fact, these two peaks seem to compete with each other

* See ESI† for conversion of Langmuirs to monolayers

View Article Online
DOI: 10.1039/C6CP01787H

displaying unpredictable outcomes such as the dominance of peak A over the peak B and *vice versa* with no clear dependence on the coverage and experimental conditions. It should be noted that occasional variation of heating ramp cannot explain the data. We encourage the reader to look at the ESI† for a detailed description of this phenomenon.

In order to address the apparent lack of reproducibility of the data and obtain a consistent set of TPD traces (Fig. 1), a large number of experiments and replications were, in fact, required. Noting that CH_3OH desorption is negligible up to 150 K, peak A displays kinetics close to zero-order having almost coincident leading edges and with its maximum shifting towards higher temperatures with increasing exposure. This peak hints to a weak C_6H_6/CH_3OH interaction. A nearly zero-order kinetics implies that the desorption rate does not depend on the C_6H_6 dose and that the interactions between the adsorbates are enthalpically favoured. Given the very low exposures reported in Fig. 1, less than an equivalent monolayer, the observed behaviour suggests that island formations, and hence dewetting of the CH_3OH substrate is already important at such low coverages. This kind of observed desorption behaviour is somewhat reminiscent of previous TPD data for C_6H_6 on compact ASW[51] where deviation from first order kinetics are observed. This also suggests a similar growth mechanism, such as island formation, and supporting the idea that small amounts of C_6H_6 exhibit some degree of interaction with the underlying H_2O and CH_3OH surface.

Peak B develops in a different and more dynamic scenario: CH_3OH desorption is no longer negligible and, as the underlying ice sublimes, structural rearrangements (*e.g.* reorientation of a CH_3OH molecule at the C_6H_6 interface) might lead to more effective interactions with the adsorbed C_6H_6. Therefore, the high temperature peak is assigned to C_6H_6 molecules that are strongly physisorbed to the CH_3OH substrate. However, this process establishing stronger interaction between C_6H_6 and CH_3OH is not the sole process occurring at this stage. Other phenomena such as the diffusion of C_6H_6 into the underlayer, and mixing might occur while both C_6H_6 and CH_3OH desorb. To summarise, a competition between several processes is observed:

1. Desorption of C_6H_6 from weak physisorption sites of the CH_3OH ice (peak A).
2. Rearrangement of the CH_3OH underlayer as the temperature increases leading to phase transitions and establishing stronger interactions with the C_6H_6.
3. Desorption of bulk CH_3OH.
4. Desorption of C_6H_6 more strongly bound to the CH_3OH as suggested by the peak above 150 K following a kinetics close to first-order (peak B).
5. Co-desorption of CH_3OH and C_6H_6 (peak C).

It is desirable to estimate the desorption energy, E_{des}, associated to peaks A and B in Fig. 1. The TPD traces from 0.02 L to 0.5 L were chosen as most appropriate for the leading edge analysis (LEA) of peak A allowing a semi-quantitative estimate of the corresponding desorption energy as 21 ± 2 kJ mol^{-1} (see ESI† for details). It should be stressed that the temperature range of interest for the LEA partially overlaps with a particular area of the TPD plot where the acquired signal is the sum of the signal coming from the sample mounting and the substrate itself. Deconvolving the latter from the former, may have altered the desorption profile at low temperatures, where the leading edge analysis is most sensitive, and hence undermined the accuracy of our estimate (ESI†).

Since the experimental traces show no clear leading edges for peak B, the estimate of the desorption energy corresponding to this feature was obtained using the Redhead equation,[75] assuming first-order kinetics and that the activation parameters are independent of surface coverage:

$$E_{des} = RT_{max} \times \left[ln\left(\frac{\nu_1 T_{max}}{\beta}\right) - 3.64 \right] \quad (2)$$

where , E_{des} is the desorption energy in J mol^{-1}, R is the gas constant in J K^{-1} mol^{-1}, β is the heating rate (1.5 K s^{-1}), and ν_1 is the pre-exponential factor (10^{12}-10^{13} s^{-1}) for a first-order desorption. The peak temperature, T_{max}, was set as 162.3 ± 0.8 K by averaging the experimental values found for multiple sets of TPD curves (14 traces in total). This analysis yields a lower limit of 39 ± 1 kJ mol^{-1} and an upper limit of 42 ± 1 kJ mol^{-1} defining a range of values for the desorption energy of peak B (see ESI† for details), which is consistent with the desorption energy (41 ± 0.5 kJ mol^{-1}) estimated for C_6H_6 on ASW at similar exposures[51]. In this case, the authors suggest that the aromatic ring is hydrogen bonded at the ASW interface *via* dangling OH groups. If similar interactions were to exist between C_6H_6 and CH_3OH (peak B), then a significant rearrangement of the CH_3OH ice structure would be required. In solid CH_3OH, the molecules are connected with each other by forming a chain-like structure *via* the OH groups.[76] During C_6H_6 adsorption, energy must be used to break the CH_3OH hydrogen-bonding network and re-orientate a surface CH_3OH to present a pendant OH group to which the aromatic π system can hydrogen bond. This process will then be enhanced while heating the substrate during the TPD itself. In contrast, the interaction leading to peak A is due to C_6H_6 molecules interacting with the substrate where no re-structuring of the surface has occurred.

RAIR spectra of C_6H_6 adsorbed on CH_3OH were collected in order to gain a further insight about the interactions established at the C_6H_6/CH_3OH interface. Coverage dependent IR experiments probe the change of the C_6H_6 binding to the chemical

View Article Online
DOI: 10.1039/C6CP01787H

surrounding environment by looking at the evolution of vibrational modes going from the monolayer towards the multilayer. As these data are acquired isothermally at base temperature (< 110 K) significant structural changes of the CH_3OH underlayer are not expected and the low exposures of C_6H_6 employed should not impact on the ice morphology. The multilayer spectrum of 200 L of CH_3OH (see ESI†) is consistent with previously reported data,[77] and with the film being mainly amorphous. Coverage dependent RAIR spectra are shown in Fig. 2 where the focus is brought exclusively onto the CC aromatic stretching mode, $\nu(CC)_{aromatic}$, of C_6H_6 as the overlayer evolves from the sub-monolayer regime, panel a), to the multilayer, panel b). These

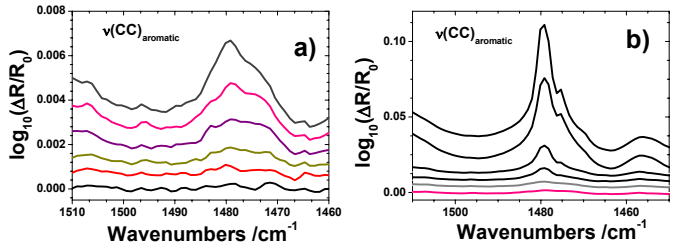

Fig. 2 RAIR spectra of C_6H_6 on thick CH_3OH film (200 L) at increasing coverages in the frequency range of interest to highlight the the CC aromatic stretching mode, $\nu(CC)_{aromatic}$ at low surface concentrations, in panel a), and at high coverages, in panel b). Spectra have been offset for clarity and subtracted from the pure CH_3OH background. C_6H_6 coverages are: 0. 1 L, 0.2 L, 0.5 L, (with a colour pattern consistent with the TPD traces), 1 L (in violet) 2 L (in pink) and 5L (in dark grey); the spectra relative to higher doses (10 L, 20 L, 50 L, and 100 L) are reported in black lines in the lower panels.

spectra were subtracted with respect to the underlying CH_3OH background as to highlight the CC aromatic stretching mode, $\nu(CC)_{aromatic}$, of C_6H_6. Although we were able to detect the in-plane (i.p) bending mode, δ(CH) i.p., at C_6H_6 exposures as low as 0.2 L the peak shape is affected by small but noticeable variations in the CO stretching mode of the underlying ice as more C_6H_6 is dosed. Other normal modes could not be detected until higher coverages were investigated ($\geq$ 5 L), and display peak maxima that are consistent with previously reported data of solid bulk C_6H_6.† [78–80] Conveniently, both the above mentioned C_6H_6 bending and stretching modes are equally sensitive to any variation of the aromaticity of the ring structure, and hence we can simply focus on the evolution CC aromatic stretch while increasing the C_6H_6 dose in order to allow a direct comparison with TPD data.

A rather broad distribution can be observed within the monolayer regime and below, for exposures as low as 0.2 L - 0.5 L as displayed in the series of IR spectra in Fig. 2a. The CC aromatic stretch mode spans over a wide range of wavenumbers ($\nu(CC)_{aromatic}$: 1465 - 1485 cm^{-1}) with a clearly discernible low frequency shoulder. These findings are consistent with the TPD results where, in a sub-monolayer regime, C_6H_6 seem to be involved in at least two different types of interactions (weak and strong) with the CH_3OH ice. The shape of the bands at low coverages in the RAIR spectra suggests the existence of multiple chemical environments, and hence possible interactions that perturb the aromaticity in the ring bonds causing the IR signatures to be broad and shifted with respect to the gas phase C_6H_6 molecule and the peak maximum of the bulk C_6H_6 (Fig. 2b). Precisely, the stretching mode displays a well-defined double peak centered at 1479 cm^{-1} and 1475 cm^{-1} at relatively high C_6H_6 exposures ($\geq$ 2 L), while this is rather flat over a wider range of frequencies up to 1 L (Fig. 2a).

3.2 TPD and RAIRS of $C_6H_6/CH_3CH_2OCH_2CH_3$

The layered binary ice comprised of C_6H_6 on $CH_3CH_2OCH_2CH_3$ cannot be effectively investigated by means of TPD. $CH_3CH_2OCH_2CH_3$ is more volatile than the aromatic species, therefore we observed that the C_6H_6 TPD peaks are largely shaped by the co-desorption with the underlayer as displayed by the striking match of the maximum and the falling edge between the desorption signal of the two species. The TPD data corresponding to very low exposures of C_6H_6 on a thick film of $CH_3CH_2OCH_2CH_3$ are displayed in Fig. 3. The low-temperature

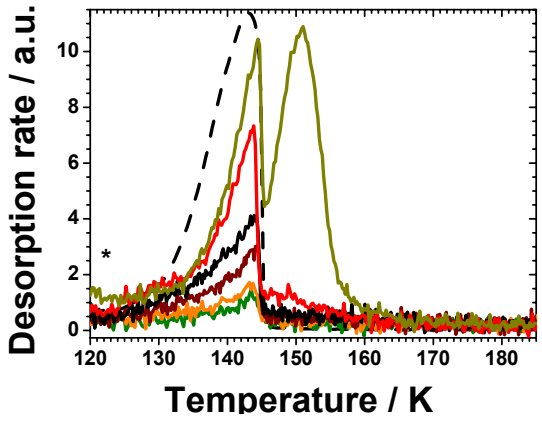

Fig. 3 TPD traces for C_6H_6 desorption from a thick ice of $CH_3CH_2OCH_2CH_3$ (200 L). C_6H_6 exposures displayed are 0.01 L in green, 0.02 L in orange, 0.05 L in brown, 0.1 L in black, 0.2 L in red, 0.5 L in dark yellow. The dashed curve represents the scaled desorption profile of $CH_3CH_2OCH_2CH_3$. The high temperature peak that is clearly distinctive in the 0.5 L trace is C_6H_6 desorbing from the stainless-steel substrate. The increase in the signal below 125 K, highlighted by the $*$ symbol, is due to undesired desorption of C_6H_6 from the sample mounting.

peak can be explained as C_6H_6 mixing with the underlayer

View Article Online
DOI: 10.1039/C6CP01787H

to subsequently desorb along with it as the ice temperature is increased, while the high temperature feature that emerges at exposures above 0.2 L of C_6H_6 can be readily assigned to C_6H_6 desorption from the metal substrate.

In contrast to the C_6H_6/CH_3OH system, the feature corresponding to the co-desorption of C_6H_6 and $CH_3CH_2OCH_2CH_3$ does not saturate in the range of exposures investigated (0.01 L - 0.5 L; 10^{-3} ML - 5×10^{-2} ML). In fact, the growth in the peak intensity as a function of the C_6H_6 coverage is somewhat reminiscent of first order desorption kinetics. Therefore, we could tentatively estimate the corresponding desorption energy using eqn (2) and choosing 143 ± 2 K as temperature of the peak maximum. Precisely, this value corresponds to the maximum for the two 0.01 L and 0.02 L traces where the trailing edge decays less abruptly. The remaining parameters are β, which was set as 0.6 K s^{-1} in agreement with the experimental conditions, and the pre-exponential, that was assumed to be 10^{12} s^{-1} as typical for a physisorbed species. It follows that E_{des} is 35 ± 1 kJ mol^{-1}. It should be stressed that such value is purely indicative though it is consistent with the desorption energy of $CH_3CH_2OCH_2CH_3$ on C_6H_6 as detailed below.

In order to investigate the behaviour of this interfacial system in a more rigorous manner, an additional set of experiments was required which consisted of depositing sub-monolayer coverages of $CH_3CH_2OCH_2CH_3$ on a thick C_6H_6 film (200 L, ~7 nm). This is shown in panel (i) of Fig. 4, where the TPD traces for (0.05 L, 0.1 L, 0.2 L, 0.5 L) $CH_3CH_2OCH_2CH_3$ from C_6H_6 are displayed. The heating ramp, β, was set as 0.80 ± 0.04 K s^{-1}. The multilayer peak begins to appear between 2 L and 5 L (ESI†). The initial sharp spike in the data (at T ~ 115 K) is an undesired signal from the sample mounting, while the most intense peak at higher temperatures is the targeted desorption peak. However, this does not decay completely to zero as the $CH_3CH_2OCH_2CH_3$ mixes with the underlying C_6H_6 during heating, which results in a broad and complex rise of the desorption signal that truncates when all the C_6H_6 is desorbed. This is similar to our observations on the C_6H_6/CH_3OH system, and although not open to quantitative analysis, it can be regarded as an evidence for dissolution of the adsorbate in the C_6H_6 matrix.

The main peak below 140 K is clearly convolved with the other two features. However, it remains the most informative about the $CH_3CH_2OCH_2CH_3C_6H_6$ interaction at the interface. In order to isolate this peak, the initial spike was subtracted from each curve. The resulting function was fitted with a convenient number of Gaussians, in order to accurately reproduce the overall trace as closely as possible, and allowing us to isolate the main TPD feature of interest. The results are consistent with first order desorption kinetics modulated by a distribution of binding energies. This clearly points to $CH_3CH_2OCH_2CH_3$ wetting the C_6H_6

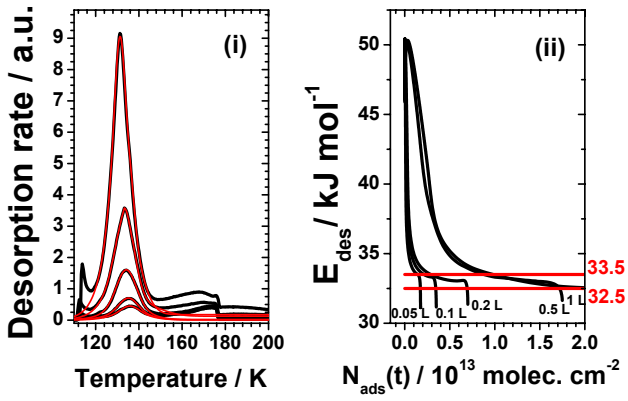

Fig. 4 Panel (i) displays the raw TPD data (in black lines) of 0.05 L, 0.1 L, 0.2 L, 0.5 L and 1 L of $CH_3CH_2OCH_2CH_3$ from 200 L of C_6H_6. The feature corresponding to the desorption of $CH_3CH_2OCH_2CH_3$ from the icy substrate is highlighted in red after subtraction of both the desorption signal from the sample mounting and the co-desorption with C_6H_6. The resulting traces were employed to derive, through inversion of the Polanyi-Wigner equation, the curves of the desorption energy, E_{des}, as a function of the surface concentration. This is shown in Panel (ii), where the average value of 33 kJ mol^{-1} was found.

surface. An alternative interpretation of the data in Fig. 4 assuming second order behaviour would imply dissociative adsorption and subsequent associative desorption. With a non-metallic interface, such as solid C_6H_6, this possibility can be discarded for physisorbed species such as $CH_3CH_2OCH_2CH_3$. Deviation from first-order behaviour with the high temperature tail have been previously reported for C_6H_6 on silica (SiO_2) by Thrower *et al.*[51] and many smaller molecules on SiO_2 and H_2O ice surfaces.[81–84] The coverage dependence of the interactions can therefore be explained in terms of (1) distribution of binding sites and/or (2) lateral repulsion between two neighbouring adsorbates.

Assuming first order kinetics, the deconvolved TPD traces can be used to give a semi-quantitative estimate of E_{des}. However, despite the good agreement with the experimental traces shown in Fig 4, care must be taken in interpreting quantitatively the data given the manipulations described. An expression of the desorption energy as a function of the surface concentration at time t, $N_{ads}(t)$, was obtained from the inversion[82,85] of the Polanyi-Wigner equation, eqn (3a), as follows:

$$r_{des} = -\frac{dN_{ads}}{dt} = \frac{\nu_1 N_{ads}}{\beta} e^{-\frac{E_{des}}{RT}} \quad (3a)$$

$$E_{des} = -RT \times ln\left(\frac{r_{des}\beta}{\nu_1 N_{ads}(t)}\right) \quad (3b)$$

View Article Online
DOI: 10.1039/C6CP01787H

where ν_1 is the pre-exponential factor for a first order desorption and was set to be 10^{12} s^{-1}, which is typical of physisorbed species.[86] However a value of 10^{13} s^{-1}, as for peak B in Fig. 1, was also tested. The initial surface coverage was estimated as per eqn (1) without dividing by the density ρ_S. and the resulting value was employed to normalise the signal at the mass spectrometer. This allows us to calculate $N_{ads}(t)$ at each time t of the TPD by subtracting the partially integrated peak area to the initial surface concentration.

The resulting curves are shown in panel (ii) of Fig. 4. The unusual behaviour at low coverages for the curves at 0.5 L and 1 L of $CH_3CH_2OCH_2CH_3$ with respect to the remaining functions can be attributed to complications arising from mixing at high temperatures and an ill-defined fit of the trailing and leading edges in the TPD. Nevertheless, the results of this analysis indicate the presence of a small distribution of desorption energies, with a mean value of 33.0 $\pm$ 1.0 kJ mol^{-1} (if $\nu_1 = 10^{13}$ s^{-1}, E_{des} = 35.5 $\pm$ 1.0 kJ mol^{-1}), corresponding to the plateau defined by the calculated curves. This result nicely matches the tentative estimate of the desorption energy found for the low temperature peak in Fig. 3 (35 $\pm$ 1 kJ mol^{-1}) and the value obtained for the second layer of $CH_3CH_2OCH_2CH_3$ on amorphous silica (35 - 32 kJ mol^{-1}).[87,88] Although the energetics at the interface of $C_6H_6/CH_3CH_2OCH_2CH_3$ ices should be regarded only as indicative, it can be concluded at least qualitatively that the C_6H_6 interface behaves with respect to the adsorbate as a surrogate of $CH_3CH_2OCH_2CH_3$ first layer. The semi-quantitative analysis of the TPD data suggests that C_6H_6 and $CH_3CH_2OCH_2CH_3$ are very much alike, thus easily mix, and that the inter-species interactions are similar to those established in the pure solids.

In contrast to TPD experiments, RAIR spectra of C_6H_6 on $CH_3CH_2OCH_2CH_3$ at *ca.* 107 K present no obvious complications.¶ Direct comparison with the results from the analogous studies on C_6H_6/CH_3OH (Fig. 2) and C_6H_6/H_2O[29] is then possible. Focusing on the low C_6H_6 surface concentrations, all the characteristic C_6H_6 bands appear as transitioning towards the multilayer regime between 5 L and 20 L (see ESI†), with peak maxima in agreement with the reported values for relatively thick ices of C_6H_6 on CH_3OH (this work), on amorphous silica,[78] on Si(111),[79] and Al.[80] Only the ring CC stretch, $\nu(CC)_{aromatic}$, was detected at low C_6H_6 exposures as shown in Fig 5a. Starting from 1 L up to higher doses, a sharp peak at 1479 cm^{-1} with a shoulder at 1475 cm^{-1} clearly grows from the background. It is noticeable that this vibrational mode exhibits a narrow line profile over the 1473 - 1481 cm^{-1} range. This clearly contrasts with C_6H_6 on CH_3OH, where this band spans over a wider range of

¶ The RAIR spectrum of the pure thick film of $CH_3CH_2OCH_2CH_3$ is discussed in the ESI†.

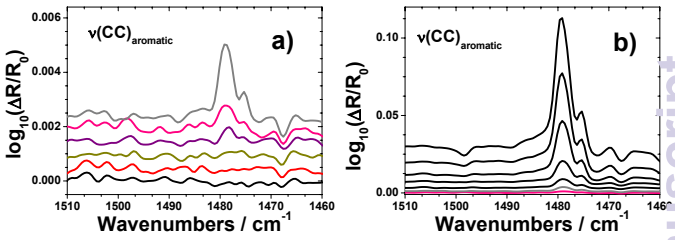

Fig. 5 RAIR spectra of C_6H_6 on thick $CH_3CH_2OCH_2CH_3$ film (200 L) at increasing C_6H_6 coverages in the frequency range of interest to highlight the CC aromatic stretching mode, $\nu(CC)aromatic$ at low surface concentrations, in panels a), and at high coverages, in panel b). Spectra have been offset for clarity and subtracted from the pure $CH_3CH_2OCH_2CH_3$ background. C_6H_6 exposures are: 0. 1 L (in black), 0.2 L (in red), 0.5 L (in dark yellow), 1 L (in violet), 2 L (in pink) and 5L (in dark grey); 10 L, 20 L, 50 L, 100 L, and 200 L (which are reported in black lines).

wavenumbers (1465 - 1485 cm^{-1}) at equivalent exposures. Indeed only above 5 L (Fig. 5b), does the band profile becomes similar, although not identical, for both the binary layered systems C_6H_6/CH_3OH and $C_6H_6/CH_3CH_2OCH_2CH_3$.

The RAIR results are in agreement with the TPD analysis in the previous paragraphs; C_6H_6 has an affinity for $CH_3CH_2OCH_2CH_3$, and hence de-wetting of $CH_3CH_2OCH_2CH_3$ from C_6H_6 does not occur. The changes in the thermodynamics (E_{des} and multibody interactions) at the interface of the layered system are not as marked as no band frequency significant shifts are detectable in the series of RAIR spectra as the C_6H_6 film grows. Conversely, a CH_3OH substrate offers a more variegated interface to the C_6H_6, allowing this to be strongly hydrogen bonded to OH groups, or interact with weak adsorption sites, *via* the CH_3 groups and the O-atoms, as displayed by the TPD data and by the broad width of the aromatic CC stretch. An additional comparison can be made with C_6H_6 on thick ASW. There island formation is the dominant process, but hydrogen bonding interactions between the π-system of the C_6H_6 ring and H_2O molecules, *via* dangling OH groups, are indicated to be responsible of the binding at the interface[29,51] with some evidence of small bathochromic shifts in peak position of the aromatic CC stretch from that of bulk C_6H_6.

3.3 Calculations and comparison with C_6H_6/H_2O

An accurate and detailed description of the investigated systems modelling hundreds of molecules is beyond the scope of this work and not feasible at the level of theory employed in this work. We chose to perform relatively high level QM calculations to carry out a consistent analysis on simple complexes of two species and small clusters of three, four molecules, in order to highlight the type of intermolecular forces in play and to confirm the thermo-

View Article Online
DOI: 10.1039/C6CP01787H

dynamics and trends observed in solid phase by TPD and RAIR experiments.

A systematic study of the main possible orientations for the complexes allowed us to find two energy minima for the following pair of species (Fig. 6), regardless of the initial input geometry: C_6H_6-H_2O, C_6H_6-CH_3OH, C_6H_6-CH_3OCH_3, C_6H_6-$CH_3CH_2OCH_2CH_3$. The corresponding binding energies are listed

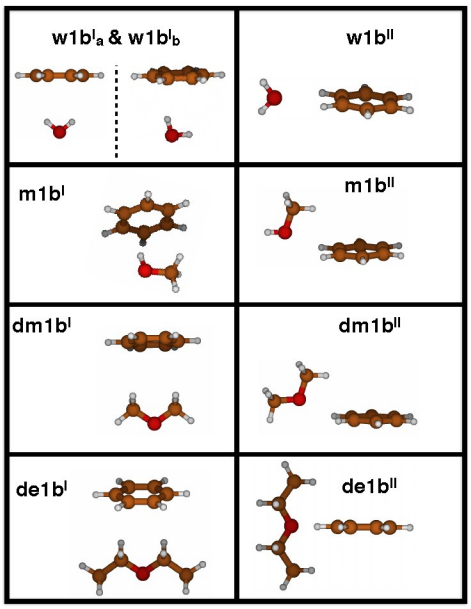

Fig. 6 Energy minima for the series of two-molecule complexes. Geometry optimisations were performed at MP2/auc-cc-pVDZ level with CP corrections.

in Table 1 and were obtained as difference of the energy of the complex and the energy of the fragments at the geometry of the complex itself ($E_{complex} - E_i - E_j$, where i and j indicate the two fragments). The agreement with previously reported data is rather good and within 1 kJ mol^{-1}, with the only exception made for $w1b''$ that can be ascribed to differences in the equilibrium geometries and in the theoretical approaches employed. The two main configurations found for each complex in Fig. 6 correspond to two types of interactions: 1) the aromatic ring acting exclusively as a hydrogen-bonding "acceptor" with its π-electron cloud (OH$\cdots\pi$; CH$\cdots\pi$) or 2) acting also as a "donor" through the edge of the ring (CH$\cdots$O). It is interesting to note that the former case is found in the global minimum for the pairs containing H_2O or CH_3OH ($w1b'_a$, $w1b'_b$ and $m1b'$), while both CH_3OCH_3 and $CH_3CH_2OCH_2CH_3$ interact more strongly with the C_6H_6 fragment when the aromatic molecule is the "donor" ($dm1b''$ and $de1b''$). However, in these two structures, along with $m1b''$, the CH$\cdots$O is not the only type of interaction that stabilises the complexes. In fact, this would be the case only for $w1b''$, where the O-atom lies in the same plane of the C_6H_6. Subsequently a substitution

Table 1 List of calculated binding energies (in kJ mol^{-1}). Literature values are also reported, when available, for comparison. $E_{MP2/TZ}$ is the BSSE corrected binding energy obtained with a single point at MP2/aug-cc-pVTZ following the optimisation with aug-cc-pVDZ basis set. E* is the BSSE corrected binding energy obtained taking into account the correction energy term, ΔCCSD(T), as E(MP2/TZ) + ΔCCSD(T).

Complex	$E_{MP2/TZ}$/kJ mol^{-1}	E*/kJ mol^{-1}	E(Lit.)/kJ mol^{-1}
$w1b'_a$	-14.0	-12.7	-11.6;[66] -12.0;[32] -14.9[89]
$w1b'_b$	-14.3	-12.9	-13.2[66]
$w1b''$	-7.0	-6.7	-5.0;[31] -3.9[74]
$m1b'$	-19.2	-16.8	-18.8[11]
$m1b''$	-11.5	-10.5	-10.9[11]
$dm1b'$	-10.9	-9.4	-9.0[37]
$dm1b''$	-12.0	-11.0	n/a
$de1b'$	-12.3	-10.4	n/a
$de1b''$	-15.5	-13.9	n/a

of the H-atom with a methyl (CH_3) group one could imagine the $w1b''$ complex to evolve into $m1b''$, where the O-atom is no longer on the same plane as the aromatic ring because of the additional CH$\cdots\pi$ interaction that further stabilises the structure. This is also observed for $dm1b''$, and, not surprisingly, in both the cases the distances between the CH_3 group and the C-atom in the ring, d(H_{CH_3}-C_{ring}) is of 3.0 Å. Moving to $de1b''$, the aliphatic chains are long enough to reach both the two ring faces (d(H_{CH_3}-C_{ring} = 3.2 Å), without moving the O-atom away from the C_6H_6 plane. Furthermore, by subtracting the binding energy, E*, of $m1b''$ or $dm1b''$ from $w1b''$, it is possible to obtain an estimate for the CH$\cdots\pi$ interaction (3.8 and 4.3 kJ mol^{-1} respectively), which is roughly the half of the difference in the binding energy between $de1b''$ and $w1b''$, 7.2 kJ mol^{-1}.

The global minimum for C_6H_6/H_2O is generally found when the H_2O molecule orientates the two H-atoms toward the π-electron density of the aromatic ring.[31,32,66,74] Looking at the complexes in the first column of Fig. 6, our results give two structures that can be regarded as energetically similar ($w1b'_a$ and $w1b'_b$) and that differ only in the tilting angle of H_2O, which is defined as the angle between the C2 axis of H_2O and the C6 axis of C_6H_6.[32] When considering $m1b'$, the interaction with the aromatic molecule increases with respect to $w1b'_a$, and the energy difference is of 3.9 kJ mol^{-1} which is due to CH$\cdots\pi$ contribution already discussed above. In fact, in this case it is not just the OH to be oriented towards C_6H_6, but also the CH_3 group that points two H-atoms towards to carbonic centres in the ring (d(H_{CH_3}-C_{ring}) = 3.2 Å).

With the C_6H_6-$CH_3CH_2OCH_2CH_3$ structure, it should be stressed that the $CH_3CH_2OCH_2CH_3$ molecule can lie under the aromatic species with two different orientations depending on the oxygen pointing away or towards the ring. Furthermore, in each of these cases the C-O bonds can align with the C-H bond

View Article Online
DOI: 10.1039/C6CP01787H

of C_6H_6 (eclipsed conformer) or can be perpendicular to it (staggered). Previous work on CH_3OCH_3 and C_6H_6 found that the difference in the binding energy between the staggered and the eclipsed orientations is negligible, less than 0.1 kJ mol^{-1}.[37] On the other hand a drastic change is seen when the O atom is pointing away or towards the C_6H_6, with E^* changing from 9.0 to 3.2 kJ mol^{-1}. Since $CH_3CH_2OCH_2CH_3$ is expected to interact with C_6H_6 in a similar way as its smaller analogue does, we chose to focus only on the more energetically stable complex, *de*1*b*′ in Fig. 6. In conclusion, all the structures are stabilised by hydrogen-bond interactions ranging between 16.8 and 6.7 kJ mol^{-1} (19.2 and 7.0 kJ mol^{-1} at MP2 level), as displayed in Table 1, with values sometimes close to the lowest minima of the C_6H_6 dimer corresponding to 13.5 and 18.1 kJ mol^{-1} which were calculated at the same level of theory (MP2/aug-cc-pVTZ)].[90] The second of the binding energies estimated for $(C_6H_6)_2$ is larger than all those calculated for all the pairs with H_2O. Therefore, on the basis of the investigation of these simple, two-molecule systems, C_6H_6-C_6H_6 interactions are more favourable than the hydrogen bonding in H_2O-C_6H_6 which is in agreement with the TPD data of Thrower *et al.*[51] that display C_6H_6 de-wetting of the ASW surface. However, the local minimum of $(C_6H_6)_2$ is comparable to the global minimum of the H_2O-C_6H_6 complex indicating that hydrogen bonding between the two species can be observed.[29,51]

The CH_3OH case is less straightforward, but there is no doubt that complex *m*1*b*′ has similar energetics to the C_6H_6 dimer. The α phase of solid CH_3OH presents a film structure made of long chains of hydrogen-bonded molecules leaving no terminal OH at the vacuum interface.[76] It follows that a C_6H_6 molecule would initially interact in a similar fashion as for the structure *m*1*b*″. In this case island formation would be the driving force during the film growth as the C_6H_6-C_6H_6 binding energy is more stabilising than that in C_6H_6-CH_3OH. This is consistent with the zero-order kinetics of peak A in the TPD traces of Fig. 1. However, the experimental data also show a high temperature peak that was explained in terms of rearrangement of the underlayer ice. This would also imply a breakdown of the chain structures in favour of equally stable interactions, which cannot be explained by simply looking at pairs of molecules.

Finally, the C_6H_6-$CH_3CH_2OCH_2CH_3$ complex has a binding energy of 15.5 kJ mol^{-1} (at MP2/aug-cc-pVTZ level of theory) that is intermediate between the lowest minima of C_6H_6-C_6H_6 (13.5 - 18.1 kJ mol^{-1}) and close the binding energy for the global minimum of the $CH_3CH_2OCH_2CH_3$ dimer (13.9 kJ mol^{-1}) (ESI†). This $(CH_3CH_2OCH_2CH_3)_2$ structure was assumed to correspond to the global minimum of $(CH_3OCH_3)_2$.[6,91,92] Therefore, in agreement with the experiments reported above, these results suggest that there is not a significant variation between the intermolecular interactions established in the pure solids and those at the interface of the layered system.

Larger clusters were also investigated employing the MP2 approach (Fig. 7, Table 2). We would like to stress that in this case, we did not choose to carry a systematic analysis of all the possible conformers, which would require a more detailed study given the large number of local minima. For instance, the interaction between C_6H_6 and several (from 1 to 6) molecules of CH_3OH with the addition of the $(C_6H_6)_2(CH_3OH)_3$ has been thoroughly investigated by Matisz *et al.*[11] by optimising thousands initial geometries. Our approach is, in contrast, more simple and we aim at an immediate validation of our hypotheses and interpretation of the trends observed in the experimental data. In fact, neither of the *m*3*b*′ and *m*3*b*″ structures is the global minimum for the $(C_6H_6)(CH_3OH)_3$ cluster, but in one case there is a "closed circle" of CH_3OH molecules interacting each one with the others, while in the other cluster this "circle" is open, leaving just one free OH to bind with the C_6H_6. The binding energies between C_6H_6 and the other three molecules agree well with the TPD data: 39.3 kJ mol^{-1} is found for *m*3*b*′, while 23.9 kJ mol^{-1} is found for *m*3*b*″ (Table 2). These values remind of the difference between the

Table 2 List of calculated binding energies (in kJ mol^{-1}). The total interaction energy, E_{tot}, is also reported to allow direct comparison with literature values, when available and this was calculated as $E_{tot} = E_{complex} - \sum_n E_n$, where n indicates the number of fragments used in the CP procedure. $E_{MP2/TZ}$ is the BSSE corrected binding energy which was obtained with a single point at MP2/aug-cc-pVTZ (CP = 2) following the optimisation with aug-cc-pVDZ basis set (CP = 3 or 4). The values in brackets are the binding energies between the furthest CH_3OCH_3 molecule and the remaining CH_3OCH_3-C_6H_6 fragment. The values in square brackets are the binding energies obtained for the CH_3OCH_3 dimer (global minimum) at the same level of theory (MP2/aug-cc-pVDZ + single point with aug-cc-pVTZ).

Cluster	E_{tot}/kJ mol^{-1}	E_{tot} (Lit.)/kJ mol^{-1}	$E_{MP2/TZ}$/kJ mol^{-1}
*w*3*b*′	-85.5	-86.6[31]	-22.5 {-21.1}[89]
*w*3*b*″	-80.5	n/a	-33.28
*m*3*b*′	-81.3	n/a	-39.3
*m*3*b*″	-94.2	-90.5[11]	-23.9
*dm*2*b*′	-26.5	[-13.7]	-12.7 (-14.2)
*dm*2*b*″	-30.5	[-13.7]	-16.4 (-24.0)

desorption energy estimated for peak B (39 - 42 kJ mol^{-1}) and A (*ca.* 21 kJ mol^{-1}) respectively in Fig. 1 supporting the interpretation of the experiments. The low temperature feature is mainly due to weakly adsorbed C_6H_6, similar to *m*3*b*″, that de-wets the CH_3OH surface, however, as the substrate is heated the CH_3OH ice rearranges and some more of the hydrogen-bonded chains in the solid break and allow the CH_3OH to tilt interacting more efficiently with C_6H_6 (*m*3*b*′).

Despite this striking match in the absolute values between the calculations and the TPD analysis, we would recommend caution when comparing desorption energies, averaged macroscopic thermodynamic quantities, with binding energies of fragments in

View Article Online
DOI: 10.1039/C6CP01787H

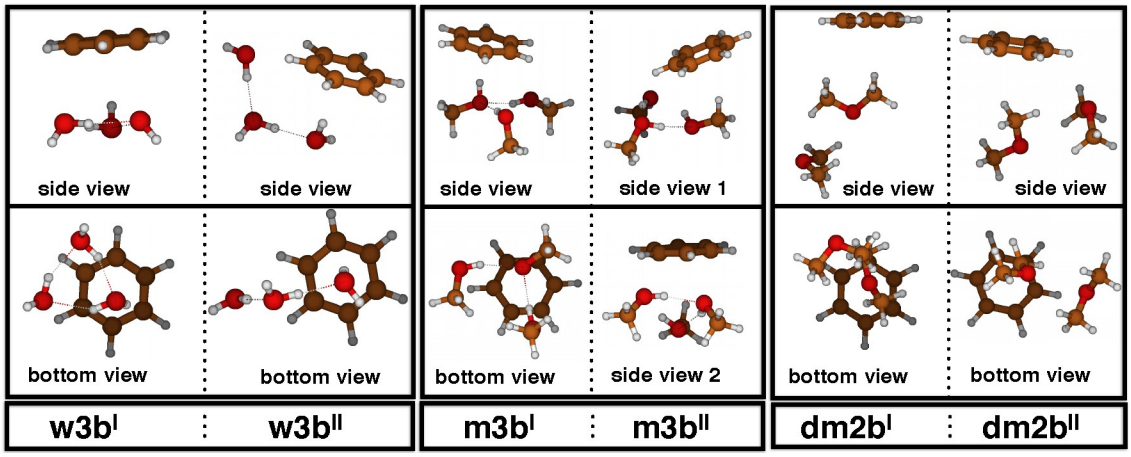

Fig. 7 Energy minima for the series of clusters. Geometry optimisations were performed at MP2/auc-cc-pVDZ level with CP correction.

small clusters. The match of these results might well be a lucky coincidence, perhaps due to some sort of compensation-effect of the errors in the analysis and in the theoretical models used (*e.g.* no zero point energy correction, overestimation of the dispersion forces in the MP2 method[31,61]). Nevertheless, these findings are promising and allow a consistent description of the investigated systems with respect to the experiments. It is interesting to note in Table 2 that $m3b'$ is the cluster which displays the strongest interaction between CH_3OH and C_6H_6 ($E_{MP2/TZ}$), but has a smaller overall interaction energy (E_{tot}) compared to $m3b''$. In particular, it follows that the OH$\cdots\pi$ interaction, as in $m3b'$, although possible, it might be less likely to be observed. This is consistent with experimental data of C_6H_6 forming islands on CH_3OH, even though evidence of strong hydrogen bonding interactions indicates some degree of surface wetting.

The clusters $w3b'$ and $w3b'$ in Fig. 7 were obtained by direct substitution of the CH_3 groups of the $m3b'$ and $m3b''$ clusters with H-atoms and re-optimised. While the circular arrangement of the CH_3OH molecules is retained by the analogous cluster with H_2O, in the other case the "circle" is broken into a chain to allow a synergic contribution of the two interactions seen in $w1b'$ and $w1b''$. Both the two structures confirm the findings reported for the smaller systems and in the literature[29–32,51,66,74,89] that C_6H_6 accepts the H-bond from the dangling OH of the H_2O cluster, and hence ASW.

In principle, especially for the C_6H_6/CH_3OCH_3 system, several configurations are energetically very similar, and a full investigation of the potential energy surface would be ideal, although computationally expensive. Therefore, we focused on two structures in particular that were obtained by adding a C_6H_6 molecule to the global minimum of the CH_3OCH_3 dimer (see ESI† for the dimer geometry[6]). With $dm2b'$ we look at how the CH$\cdots\pi$ interaction seen in $dm1b'$ changes when a second molecule of CH_3OCH_3 is added. The resulting complex does not vary much with respect to the simpler $dm1b'$ neither in the energetics nor in the overall geometry. In fact, the binding energy of the aromatic molecule with the fragment in $dm2b'$ is only 1.8 kJ mol^{-1} higher than in the smaller complex ($dm1b'$). Despite a rearrangement in the relative positions between the aromatic ring plane and the CH_3 groups, the CH$\cdots\pi$ distances remain almost unchanged (varying of maximum 0.3 Å) when comparing $dm2b'$ to $dm1b'$. Moreover, the CH$\cdots$O length in the CH_3OCH_3-CH_3OCH_3 complex, remains unaltered whether this is measured in the isolated dimer (ESI†) or in the analogous fragment in the larger $dm2b'$ cluster.

With the $dm2b''$ structure we look at the case where C_6H_6 act as hydrogen bonding donor. At first glance, in this configuration, the relative orientation between the aromatic ring and the closest CH_3OCH_3 molecule is quite different from what is found in $dm1b''$ and this can be regarded as a $\pi/2$ rotation of the C_6H_6 plane with respect to the plane defined by the C-O-C. Such rearrangement of the CH_3OCH_3 molecules around the C_6H_6 ring when compared to $dm1b''$ allows the second CH_3OCH_3 molecule to interact via its CH_3 end with the π-orbitals of C_6H_6. This results in a synergic effect of the CH$\cdots\pi$ and CH$\cdots$O interactions and the distance between the O-atom and the aromatic proton is almost identical ($\Delta d \leq 0.1$ Å) in $dm1b''$ and $dm2b''$. In conclusion, regardless of the way the aromatic ring binds with the other fragment in the two structures $dm2b'$ and $dm2b''$, the difference in the overall interaction energy term, E_{tot}, is just of 4 kJ mol^{-1}.

The binding energy between the aromatic molecule and the other fragment (12.7 and 16.4 kJ mol^{-1}) is comparable to that of the C_6H_6 dimer (13.5 and 18.1 kJ mol^{-1})[90] and of the CH_3OCH_3 dimer (13.7 kJ mol^{-1}), confirming that these two species have energetically similar intermolecular interactions. Alternatively, when looking at the binding energy between the furthest CH_3OCH_3 molecule and the remaining CH_3OCH_3-C_6H_6

View Article Online
DOI: 10.1039/C6CP01787H

fragment, the interactions are of 14.2 and 24 kJ mol^{-1} for *dm2b′* and *dm2b′* respectively. These values are still very close to those just mentioned above. In fact, in the *dm2b′* structure the aromatic ring will have only a marginal and indirect effect on the binding energy between the two CH_3OCH_3 molecules. Therefore, it is not surprising that the calculated 14.2 kJ mol^{-1} is extremely close to the 13.7 kJ mol^{-1} found in the CH_3OCH_3 dimer. Regarding the complex in *dm2b″*, it should be noted that the 24 kJ mol^{-1} value results from the synergic and direct effect of two types of interactions, CH_3OCH_3-CH_3OCH_3 and CH_3OCH_3-C_6H_6. The resulting stabilisation is roughly the sum of the binding energy in the CH_3OCH_3 dimer and in *dm1b′*, further confirming the similarity of the intermolecular interactions that are typical for the two species. These results, based on simple calculations, present an overall picture of the C_6H_6/CH_3OCH_3 system, and hence of the $C_6H_6/CH_3CH_2OCH_2CH_3$ system, that is consistent with RAIR and TPD experiments, although no quantitative comparison can be made. Therefore, the findings indicate that no changes in the thermodynamics (enthalpy) occur at the interface, and hence a uniform layer-by-layer growth of one ice over the other is expected.

4 Conclusions

We have presented a series of experiments and simple calculations to investigate the role of non-covalent interactions, *e.g.* hydrogen bonding, in determining the ice structure of binary layered systems. Table 3 summarises the growth mechanisms and the desorption energy of these ices.

Table 3 Table summarising the desorption energies and the film growth mechanisms for the following binary layered systems: C_6H_6/H_2O, C_6H_6/CH_3OH, $CH_3CH_2OCH_2CH_3/C_6H_6$ and $C_6H_6/CH_3CH_2OCH_2CH_3$. The question mark highlights a tentative determination.

Substrate	Overlayer	Film growth	E_{des}/kJ mol^{-1} (sub-monolayer)
H_2O	C_6H_6	Islanding	41.0 ±0.5 [51]
CH_3OH	C_6H_6	Islanding	21 ±2?
		Wetting	39 - 42
$CH_3CH_2OCH_2CH_3$	C_6H_6	Wetting?	35 ±1?
C_6H_6	$CH_3CH_2OCH_2CH_3$	Wetting	33 ±1

Both TPD traces and RAIR spectra of C_6H_6 on a CH_3OH ice indicate that island formation is probably the driving process during the film growth of the overlayer. Especially at low exposures, most of the isolated aromatic molecules that are directly adsorbed at the ice interface are weakly bound to the methyl groups (CH$\cdots\pi$) and to the O-atom (CH$\cdots$O), having a desorption energy of *ca.* 21 ± 2 kJ mol^{-1}. There are also considerable evidence of strong binding mainly through the hydroxyl group to the aromatic ring (OH$\cdots\pi$) corresponding to an E_{des} in the 39 - 42 kJ mol^{-1} range that implies a rearrangement of the CH_3OH chains in the substrate. This phenomenon is enhanced during TPD. In conclusion, the C_6H_6/CH_3OH interface shares more than one similarity, with the analogous layered C_6H_6/H_2O system, *e.g.* island formation and interaction through dangling OH groups.

The $C_6H_6/CH_3CH_2OCH_2CH_3$ has been the most challenging to study, pushing established surface techniques, such as TPD and RAIRS , to their limits of detection and applicability. However we found that the desorption energy corresponding to low exposures of C_6H_6 on thick $CH_3CH_2OCH_2CH_3$ ices has a tentative value of *ca.* 35 ±1 kJ mol^{-1}, which is noticeably close to the 33 ±1 kJ mol^{-1} found for the reversed system. In conclusion, although the initial interpretation of C_6H_6 wetting $CH_3CH_2OCH_2CH_3$ is based on the inverted experiment, the addition of RAIRS data and MP2 calculations support the idea that the C_6H_6 film grows uniformly on the $CH_3CH_2OCH_2CH_3$ substrate, with no significant variations between the possible intermolecular interactions in the bulk of the two solid phases and at the interface.

5 Acknowledgments

The authors would like to acknowledge the use of the EPSRC UK National Service for Computational Chemistry Software (NSCCS) at Imperial College London and contributions from its staff in carrying out this work. The authors acknowledge the support of the European Community FP7-ITN Marie-Curie Programme (LASSIE project, grant agreement #238258). Financial support from Heriot-Watt University for a number of upgrades to the UHV system is also acknowledged. DM clarifies that his contribution to this work has been done as a private venture and not in the author's capacity as an affiliate of the Jet Propulsion Laboratory, California Institute of Technology. The authors would like to thank Prof. Maciej Gutowski (Heriot-Watt University) and Dr. Enrico Ronca (Princeton University) for the very helpful discussions.

References

1 O. Takahashi, Y. Kohno and M. Nishio, *Chem. Rev.*, 2010, **110**, 6049–6076.
2 D. Cappelletti, E. Ronca, L. Belpassi, F. Tarantelli and F. Pirani, *Acc. Chem. Res.*, 2012, **45**, 1571–1580.
3 J. K. Gregory, D. C. Clary, K. Liu, M. G. Brown and R. J. Saykally, *Science*, 1997, **275**, 814–817.
4 J. Ceponkus, P. Uvdal and B. Nelander, *J. Phys. Chem. A*, 2008, **112**, 3921–3926.
5 F. Kollipost, K. Papendorf, Y.-F. Lee, Y.-P. Lee and M. A. Suhm, *Phys. Chem. Chem. Phys.*, 2014, **16**, 15948–15956.
6 Y. Tatamitani, B. Liu, J. Shimada, T. Ogata, P. Ottaviani, A. Maris, W. Caminati and J. L. Alonso, *J. Am. Chem. Soc.*, 2002, **124**, 2739–2743.
7 K. Shibasaki, A. Fujii, N. Mikami and S. Tsuzuki, *J. Phys. Chem. A*, 2006, **110**, 4397–4404.
8 L. Pauling, *The Nature of the Chemical Bond.*, Cornell University Press, Ithaca, NY, 1960.

View Article Online
DOI: 10.1039/C6CP01787H

9 M. Müller-Dethlefs and P. Hobza, *Chem. Rev.*, 2000, **100**, 143–168.
10 C.-F. Fu and S. X. Tian, *Phys. Chem. Chem. Phys.*, 2014, **16**, 21957–21963.
11 G. Matisz, A. Kelterer, W. M. F. Fabian and Kunsági-Máté, *J. Phys. Chem. A*, 2011, **115**, 10556–10564.
12 T. Steiner, *Angew. Chem. Int. Ed.*, 2002, **41**, 48–76.
13 G. R. Desiraju and T. Steiner, *The Weak Hydrogen Bond in Structural Chemistry and Biology*, Oxford University Press, New York, 2001.
14 S. K. Burley and G. A. Petsko, *Science*, 1985, **229**, 23–28.
15 T. Steiner and G. Koellner, *J. Mol. Biol.*, 2001, **305**, 535–557.
16 M. Brandl, M. S. Weiss, A. Jabs, J. Sühnel and R. Hilgenfeld, *J. Mol. Biol.*, 2001, **307**, 357–377.
17 J.-M. Lehn, *Angew. Chem., Int. Ed.*, 1988, **27**, 89–112.
18 J.-M. Lehn, *Angew. Chem., Int. Ed. Engl.*, 1990, **29**, 1304–1319.
19 W. Ji, G. Liu, Z. Li and C. Feng, *ACS Appl. Mater. Interfaces*, 2016, in print.
20 M. J. Plevin, D. L. Bryce and J. Boisbouvier, *Nat. Chem.*, 2010, **2**, 466–471.
21 P. Cysewski, *Phys. Chem. Chem. Phys.*, 2008, **10**, 2636–2645.
22 R. Carrillo, M. Lípez-Rodríguez, V. Martín and T. Martín, *Angew. Chem. Int. Ed.*, 2009, **48**, 7803–7808.
23 L. M. Salonen, M. Ellermann and F. Diederich, *Angew. Chem. Int. Ed.*, 2011, **50**, 4808–4842.
24 A. J. Gotch, A. W. Garrett, D. L. Severance and T. S. Zwier, *Chem. Phys. Lett.*, 1991, **178**, 121–129.
25 A. J. Gotch and T. S. Zwier, *J. Chem. Phys.*, 1992, **96**, 3388–3401.
26 A. J. Garrett and T. S. Zwier, *J. Chem. Phys.*, 1992, **96**, 3402–3410.
27 R. N. Pribble and T. S. Zwier, *Faraday Discuss.*, 1994, **97**, 229–241.
28 J. D. Thrower, M. P. Collings, F. J. M. Rutten and M. R. S. McCoustra, *Chem. Phys. Lett.*, 2011, **505**, 106–111.
29 D. Marchione, J. D. Thrower and M. R. S. McCoustra, *Phys. Chem. Chem. Phys.*, 2016, **18**, 4026–4034.
30 D. Sharma and M. J. Paterson, *Photochem. Photobiol. Sci.*, 2014, **13**, 1549–1560.
31 L. V. Slipchenko and M. S. Gordon, *J. Phys. Chem. A*, 2009, **113**, 2092–2102.
32 S. Li, V. R. Cooper, T. Thonhauser, A. Puzder and D. C. Langreth, *J. Phys. Chem. A*, 2008, **112**, 9031–9036.
33 D. Z. Veljković, G. V. Janjić and S. D. Zarić, *CrystEngComm*, 2011, **13**, 5005–5010.
34 D. P. Malenov, G. V. Janjić, D. Z. Veljković and S. D. Zarić, *Comput. Theor. Chem.*, 2013, **1018**, 59–65.
35 M. Albertí, A. Aguilar, J. M. Lucas and P. Pirani, *J. Phys. Chem. A*, 2012, **116**, 5480–5490.
36 M. Albertí, A. Aguilar, F. Huarte-Larrañaga, J. M. Lucas and P. Pirani, *J. Phys. Chem. A*, 2014, **118**, 1651–1662.
37 J. C. Amicangelo, I. D. G. Gung, B. W. and N. C. Romano, *Phys. Chem. Chem. Phys.*, 2008, **10**, 2695–2705.
38 B. M. Jones, F. Zhang, R. I. Kaiser, A. Jamal, A. M. Mebel, M. A. Cordiner and S. B. Charnley, *Proc. Natl. Acad. Sci. U. S. A.*, 2010, **108**, 452–457.
39 J. Cernicharo, A. M. Heras, A. Tielens, J. R. Pardo, F. Herpin, M. Guélin and L. B. F. M. Waters, *Astrophys. J.*, 2001, **546**, L123–L126.
40 V. Vuitton, R. V. Yelle and P. Lavvas, *Phil. Trans. R. Soc. A*, 2009, **367**, 729–741.
41 M. L. Delitsky and C. P. McKay, *Icarus*, 2010, **207**, 477–484.
42 H. Bockhorn, F. Fitting, H. W. Wenz and B. Bunsenges, *Ber. Bunsenges. Phys. Chem.*, 1984, **20**, 1067–1073.
43 M. Frenklach, D. W. Clary, W. C. Gardiner and S. E. Stein, *Proc. Combust. Inst.*, 1984, **20**, 887–901.
44 A. G. G. M. Tielens, *Rev. Mod. Phys.*, 2013, **85**, 1021–1081.
45 P. Merino, M. Švec, J. I. Martinez, P. Jelinek, P. Lacovig, M. Dalmiglio, S. Lizzit, P. Soukiassian, J. Cernicharo and J. A. Martin-Gago, *Nat. Commun.*, 2014, **5**, 1–9.
46 K. I. Öberg, A. C. A. Boogert, K. M. Pontoppidan, S. van den Broek, E. F. van Dishoeck, B. Sandrine, A. B. Geoffrey and N. J. Evans II, *Astrophys. J.*, 2011, **740**, 109.
47 I. Medvedev, M. Winnewisser, F. C. De Lucia, E. Herbst, E. Yi, L. P. Leong, R. P. A. Bettens, E. Biankowska-Jaworska, O. Desyatnyk, L. Pszczónkowski and Z. Kisiel, *Astrophys. J. Suppl. Ser.*, 2003, **148**, 593–597.
48 S. C. Silva and J. P. Devlin, *J. Phys. Chem.*, 1994, **98**, 10847–10852.
49 R. Souda, *J. Phys. Chem. B*, 2004, **108**, 283–288.
50 S. Bahr and V. Kempter, *J. Chem. Phys.*, 2007, **127**, 074707.
51 J. D. Thrower, M. P. Collings, F. J. M. Rutten and M. R. S. McCoustra, *J. Chem. Phys.*, 2009, **131**, 244711.
52 D. Marchione and M. R. S. McCoustra, *in preparation*.
53 J. D. Thrower, M. P. Collings, F. J. M. Rutten and M. R. S. McCoustra, *Mon. Not. R. Astron. Soc.*, 2009, **394**, 1510–1518.
54 R. L. Summers, *Empirical observations on the sensitivity of hot cathode ionization type vacuum gauges*, National Aeronautics and Space Administration, Washington, D. C., 1969.
55 J. E. Bartmess and M. Georgiadis, R, *Vacuum*, 1983, **33**, 149–153.
56 M. Schulte, B. Schlosser and W. Seidel, *Fresenius J. Anal. Chem.*, 1994, **348**, 778–780.
57 G. D. Waddill and L. L. Kesmodel, *Phys. Rev. B*, 1985, **31**, 4940–4946.

View Article Online
DOI: 10.1039/C6CP01787H

58 S. D. Green, A. S. Bolina, R. Chen, M. P. Collings, W. A. Brown and M. R. S. McCoustra, *Mon. Not. R. Astron. Soc.*, 2009, **398**, 357.

59 C. J. Craven, P. D. Hatton, C. J. Howard and G. S. Pawley, *J. Chem. Phys.*, 1993, **98**, 8236–8243.

60 M. J. Frisch, G. W. Trucks, H. B. Schlegel, G. E. Scuseria, M. A. Robb, J. R. Cheeseman, G. Scalmani, V. Barone, B. Mennucci, G. A. Petersson, H. Nakatsuji, M. Caricato, X. Li, H. P. Hratchian, A. F. Izmaylov, J. Bloino, G. Zheng, J. L. Sonnenberg, M. Hada, M. Ehara, K. Toyota, R. Fukuda, J. Hasegawa, M. Ishida, T. Nakajima, Y. Honda, O. Kitao, H. Nakai, T. Vreven, J. A. Montgomery, Jr., J. E. Peralta, F. Ogliaro, M. Bearpark, J. J. Heyd, E. Brothers, K. N. Kudin, V. N. Staroverov, R. Kobayashi, J. Normand, K. Raghavachari, A. Rendell, J. C. Burant, S. S. Iyengar, J. Tomasi, M. Cossi, N. Rega, J. M. Millam, M. Klene, J. E. Knox, J. B. Cross, V. Bakken, C. Adamo, J. Jaramillo, R. Gomperts, R. E. Stratmann, O. Yazyev, A. J. Austin, R. Cammi, C. Pomelli, J. W. Ochterski, R. L. Martin, K. Morokuma, V. G. Zakrzewski, G. A. Voth, P. Salvador, J. J. Dannenberg, S. Dapprich, A. D. Daniels, Ã. Farkas, J. B. Foresman, J. V. Ortiz, J. Cioslowski and D. J. Fox, *Gaussian09 Revision D.01*, Gaussian Inc. Wallingford CT 2009.

61 C. Møller and M. S. Plesset, *Phys. Rev.*, 1934, **46**, 618–622.

62 M. Head-Gordon, J. A. Pople and M. J. Frisch, *Chem. Phys. Lett.*, 1988, **153**, 503–506.

63 T. H. Dunning, *J. Chem. Phys.*, 1989, **90**, 1007–1023.

64 R. A. Kendall, T. H. Dunning and R. J. Harrison, *J. Chem. Phys.*, 1992, **96**, 6796–6806.

65 D. E. Woon and T. H. Dunning, *J. Chem. Phys.*, 1993, **98**, 1358–1371.

66 S. Tsuzuki, K. Honda, T. Uchimaru, M. Mikami and K. Tanabe, *J. Am. Chem. Soc.*, 2000, **122**, 11450–11458.

67 S. F. Boys and R. Bernardi, *Mol. Phys.*, 1970, **19**, 533–566.

68 F. B. van Duijneveldt, J. G. C. M. van Duijneveldt-van de Rijdt and J. H. van Lenthe, *Chem. Rev.*, 1994, **94**, 1873–1885.

69 G. Schaftenaar and J. H. Noordik, *J. Comput. Aided Mol. Des.*, 2000, **14**, 123–134.

70 K. Lum, D. Chandler and J. D. Weeks, *J. Phys. Chem. B*, 1999, **103**, 4570–4577.

71 D. Chandler, *Nature*, 2005, **437**, 640–647.

72 S. Rajamani, T. M. Truskett and S. Garde, *Proc. Natl. Acad. Sci. USA*, 2005, **102**, 9475–9480.

73 J. Mittal and G. Hummer, *Proc. Natl. Acad. Sci. USA*, 2008, **105**, 20130–20135.

74 M. Albertí, N. F. Lago and F. Pirani, *Chem. Phys.*, 2012, **399**, 232–239.

75 P. A. Redhead, *Vacuum*, 1962, **12**, 203–211.

76 O. Gálvez, B. Maté, B. Martín-Llorente, V. J. Herrero and R. Escribano, *J. Phys. Chem. A*, 2009, **113**, 3321–3329.

77 A. S. Bolina, A. J. Wolff and W. A. Brown, *J. Chem. Phys.*, 2005, **122**, 044713.

78 J. D. Thrower, *PhD thesis*, Heriot-Watt University, 2009.

79 G. Strazzulla and G. A. Baratta, *Astron. Astrophys.*, 1991, **241**, 310–316.

80 R. Ruiterkamp, Z. Peeters, M. H. Moore, R. L. Hudson and P. Ehrenfreund, *Astron. Astrophys.*, 2005, **440**, 391–402.

81 M. P. Collings, J. W. Dever, H. J. Fraser and M. R. S. McCoustra, *Astrophys. Space Sci.*, 2003, **285**, 633–659.

82 T. Zubkov, R. S. Smith, T. R. Engstrom and B. D. Kay, *J. Chem. Phys.*, 2007, **127**, 184707.

83 L. Hornekær, A. Baurichter, V. V. Petrunin, A. C. Luntz, D. B. Kay and A. Al-Halabi, *J. Chem. Phys.*, 2005, **122**, 124701.

84 L. Amiaud, F. Dulieu, H. H. Fillion, A. Momeni and J. L. Lemaire, *J. Chem. Phys.*, 2007, **127**, 144709.

85 S. L. Tait, Z. Dohnálek, C. T. Campbell and B. D. Kay, *J. Chem Phys.*, 2005, **122**, 164707.

86 M. P. Collings, V. L. Frankland, J. Lasne, D. Marchione, A. Rosu-Finsen and M. R. S. McCoustra, *Mon. Not. R. Astron. Soc.*, 2015, **449**, 1826–1833.

87 D. Marchione, *PhD thesis*, Heriot-Watt University, 2015.

88 D. Marchione, A. Rosu-Finsen and M. R. S. McCoustra, *in preparation*.

89 M. Prakash, K. G. Samy and V. Subramanian, *J. Phys. Chem. A*, 2009, **113**, 13845–13852.

90 J. G. Hill, J. A. Platts and H. J. Werner, *Phys. Chem. Chem. Phys.*, 2006, **8**, 4072–4078.

91 A. Karpfen and E. S. Kryachko, *Phys. Chem. Lett.*, 2006, **431**, 428–433.

92 B. L. Yoder, K. B. Bravaya, A. Bodi, A. H. C. West, B. Sztáray and R. Signorell, *J. Chem. Phys.*, 2015, **142**, 114303–1.